IEEE Photonics Journal
An IEEE Photonics Society Publication

Absolute Electroluminescence Imaging Diagnosis of GaAs Thin-Film Solar Cells

Volume 9, Number 5, October 2017

XiaoBo Hu
Tengfei Chen
Juanjuan Xue
Guoen Weng
Shaoqiang Chen
Hidefumi Akiyama
Ziqiang Zhu

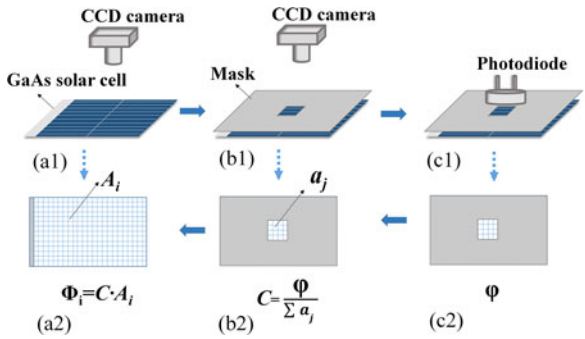

DOI: 10.1109/JPHOT.2017.2731800
1943-0655

Absolute Electroluminescence Imaging Diagnosis of GaAs Thin-Film Solar Cells

XiaoBo Hu,[1] Tengfei Chen,[1] Juanjuan Xue,[1] Guoen Weng,[1] Shaoqiang Chen,[1] Hidefumi Akiyama,[2,4] and Ziqiang Zhu[3]

[1]Department of Electronic Engineering, East China Normal University, Shanghai 200241, China
[2]Institute for Solid State Physics, The University of Tokyo, Chiba 2778581, Japan
[3]East China Normal University, Shanghai 200241, China
[4]AIST-UTokyo Advanced Operando-Measurement Technology Open Innovation Laboratory, Chiba 2778589, Japan

DOI:10.1109/JPHOT.2017.2731800

Manuscript received May 6, 2017; revised July 15, 2017; accepted July 21, 2017. Date of publication July 26, 2017; date of current version October 6, 2017. This work was supported in part by the Recruitment Program of Global Experts (1000 Talent Plan) of China, in part by the Natural National Science Foundation of China (61604055), in part by the Shanghai Pujiang Program (16PJ1402600) in China, in part by the KAKENHI No. 15H03968 and No. 26390075 from JSPS, and in part by the Photon Frontier Network Program of MEXT, OPERANDO-OIL, and NEDO in Japan. Corresponding author: Shaoqiang Chen (e-mail: sqchen@ee.ecnu.edu.cn).

Abstract: A spatially resolved absolute electroluminescence (EL) imaging method was utilized to analyze the photovoltaic properties and resistive loss properties of a GaAs thin-film solar cell. The *I–V* relation was extrapolated from the absolute EL efficiency measurements in conjunction with the external-quantum-efficiency (EQE) measurements; the EL extrapolated *I–V* relation has a merit over the conventional *I–V* relation measured with a solar simulator that it could eliminate the series resistance effect caused by external probe contact. Then, the mapping of the internal voltage of the solar cell and the sheet resistance of the window layer of the solar cell were obtained from the calibrated absolute EL imaging method. Finally, optic electroconversion losses of the solar cell including radiative loss, nonradiative loss, thermalization loss, transmission loss, and junction loss were quantified given by the EL and EQE measurements.

Index Terms: Luminiescence and fluorescence, imaging systems.

1. Introduction

Electroluminescence (EL) measurement is a powerful tool to characterize solar cells which has gained much attention recently [1]–[13]. By measuring the spatial distribution of the EL intensity from the top surface of solar cells, it is easy to find failures from the EL images such as electrode faults and cell cracks which has been used in maximizing module manufacturing yields such as in crystalline silicon cells [7]–[10]. Furthermore, it is possible to extract spatially resolved information about the electronic material properties of solar cells such as minority-carrier diffusion length, diode performance, series resistance, shunts and local junction voltage from the EL images [7]–[24]. Recently, an absolute EL method [25] has been demonstrated to characterize solar cells which is based on the basic reciprocity relationship [15], [16] between EL emission in light-emitting-diode (LED) operation and the external quantum efficiency (EQE) in solar-cell operation. This method involves in obtaining measurements of the absolute EL intensity to directly evaluate the internal

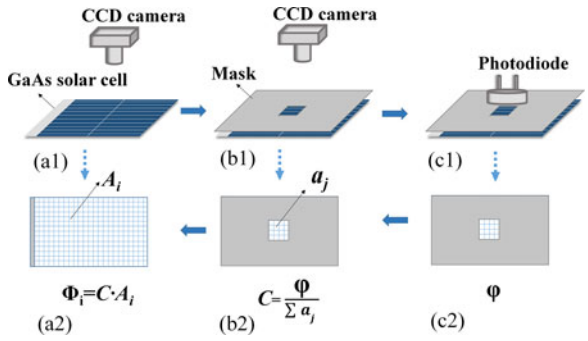

Fig. 1. The schematic of the experimental setup for the absolutely calibrated EL measurements of the GaAs solar cell.

current-voltage (I-V) properties of solar cells, and no extra parametric adjustments or fittings are necessary [25]. Based on this method, an absolute EL imaging method has been developed to quantitative mapping the open-circuit voltage of Si solar cells and modules [26]. However, both of the work [25], [26] made an assumption which considered the properties of the solar cells were spatially uniform on the surface. However, practical solar cells have more or less spatial inhomogeneity [27] and a more accurate method is necessary.

In this study, an absolutely calibrated electroluminescence imaging method was proposed which also considered the inhomogeneity over the surface of the solar cell. Based on the method, the mapping of the internal voltage of the solar cell, the sheet resistance of the window-layer of the solar cell were obtained. While in conjunction with the EQE measurements, the I-V properties and the quantitative optic-electro losses were also obtained.

2. Experimental Details

In this study, a mono-crystalline GaAs solar cell was used as the testing sample. The total area of the solar cell is $4 \times 2\,cm^2$. Fig. 1 shows the schematic of the experimental setup for the absolutely calibrated EL measurements of the GaAs solar cell. In Fig. 1(a1), a silicon charge-coupled device (CCD) camera with 4800×6400 pixels was set above the solar cell to measure the EL images of the solar cell. The forward current was injected by a current-voltage source. The exposure time of the CCD varied from 20 ms to 2 s depending on the injection current. Then in Fig. 1(b1), a mask was put closely above the cell which only allow part of the EL emitted from the cell surface to pass through and measured by the CCD camera. The shape of the transparent part of the mask was designed to be square with a side length of 0.5 cm. Then, a calibrated Si photodiode was put above the transparent part of the mask in Fig. 1(b1) in the face-to-face geometry as Fig. 1(c1) shows to measure the absolute EL power. The shape of the effective area of the Si photodiode is a circle with a diameter of 0.85 cm which could totally cover the transparent part of the mask. The absolute EL power was measured and denoted by φ (photon flux) as Fig. 1(c2) shows. The EL intensity measured by CCD is a relative quantity, the EL intensity of each pixel measured by CCD is denoted by a_j as Fig. 1(b2) shows. Then a calibrated constant C was defined which could calibrate the EL intensity measured by CCD to an absolute intensity, then we have $C = \varphi / \sum a_j$ as Fig. 1(b2) shows. Finally, the absolute EL intensity of each pixel Φ_i (photon flux) could be calibrated to be $\Phi_i = C \cdot A_i$, where A_i is the EL intensity of each pixel measured by CCD before calibration.

The I-V curve of the GaAs solar cell was measured under AM1.5G, 1-sun illumination condition using a solar simulator at room temperature. The short-circuit current density (J_{sc}) was 25.3 mA/cm^2, the open-circuit voltage (V_{oc}) was 0.996 V, and the energy conversion efficiency (η) was 19.4%. The EQE of the solar cell was measured by a quantum efficiency measurement system (ORIEL IQE200, Newport Corp.) where the excitation spot radius of the EQE measurement was 0.8 mm, and the spot was positioned at the cell center to ensure that the cell electrodes were avoided. The

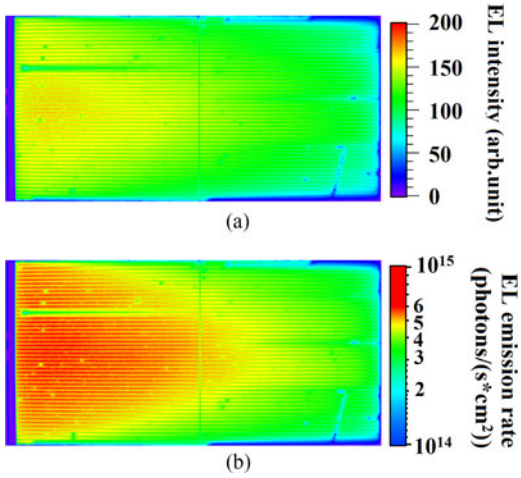

Fig. 2. EL image measured by CCD camera before calibration with relative EL intensity (a); and after calibration with absolute EL emission rate (b).

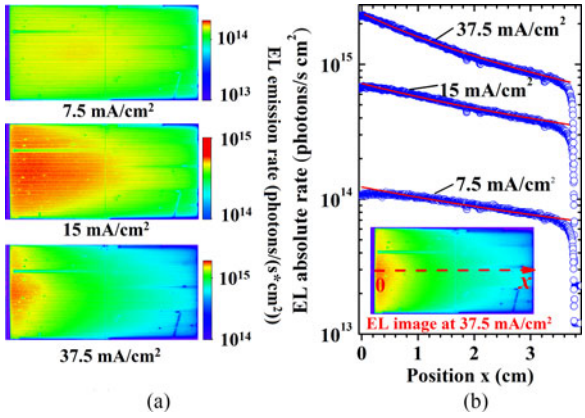

Fig. 3. (a) Images of the absolute EL intensity of GaAs solar cell under different forward injection current density. (b) Horizontal line scans of the absolute EL intensity (blue circle lines) across the cell (x-direction) as shown by the inset, the red solid lines are the the fitting results.

EL spectra was measured by a fiber probe connected to a spectrometer which is composed of a monochromator and a cooled silicon charge-coupled device (CCD).

3. Results and Discussions

Fig. 2(a) shows the EL image with forward injection current of 15 mA/cm^2 measured by CCD camera without calibration with EL intensity of arbitrary unit; Fig. 2(b) shows the calibrated image of the absolute EL emission rate with unit of photons/(s·cm^2) based on the steps illustrated in Fig. 1. It can be seen from Fig. 2(b) that the maximum difference of the absolute EL intensity is about 1 order and many small local defects could be seen which indicate the inhomogeneity of the solar cell.

Fig. 3(a) shows the image of the absolute EL intensity of the GaAs solar cell under various injection current density, it is obviously to see that higher injection current density leads to higher EL emission intensity. Fig. 3(b) shows the absolute EL intensity across the cell along the *x*-direction (as the dash arrow shows in the inset) for three different forward injection current densities. It could be seen that the EL intensity gradually decreased along the *x*-direction for all current densities. It is

easy to understand this point since as the distance from the left current injection electrode gradually increased along the *x*-direction, the voltage $V(x)$ gradually decreased due to the resistance effect of the top p-GaAs layer and thus leading the EL intensity also decreased. G. T. Koishiyev [28] proposed a lateral current model which included the sheet resistance of the top layer ρ to illustrate the decreasing of the EL intensity along the *x*-direction as follows,

$$\frac{\phi(x)}{\phi(0)} = \left\{1 + \frac{I\beta\rho}{2}\left(\frac{L}{W}\right)\left[1 - \left(1 - \frac{x}{L}\right)^2\right]\right\}^{-A} \tag{1}$$

where ϕ is the EL intensity, I is the total injection current (mA), $\beta = q/AkT$ and A is the diode quality factor. L and W are the cell length (*x*-direction) and width respectively. The red solid line shows the fitting result by using (1) which considered a sheet resistance ρ of the p-GaAs top layer with the value of (0.1 $\pm$ 0.02) $\Omega/\square$ and the diode quality factor A with the value of (1.8 $\pm$ 0.05).

According to the reciprocity theorem established by U. Rau [15], the EL intensity ϕ_{emi} (photons/(s·cm^2)) of a solar cell emitted at any position "*i*" (the CCD camera pixel) from the solar cell's surface is given by

$$\phi_{emi}(E) = Q_{ei}(E)\phi_{bb}(E)\exp\left(\frac{qV_i}{kT}\right) \tag{2}$$

where $Q_{ei}(E)$ is the EQE of the solar cell, E is the photon energy, q is the elementary charge, k is the Boltzmann constant and T is the Kelvin temperature, V_i is the internal junction voltage and ϕ_{bb} is the spectral photon density of a black body, which depends on Planck's constant h and the vacuum speed c of light, which is given by

$$\phi_{bb}(E) = \frac{2\pi E^2}{h^3c^2}\exp\left(-\frac{E}{kT}\right) \tag{3}$$

Thus, the internal voltage V_i of each pixel could be obtained based on (1) as following shows,

$$V_i = \frac{kT}{q}\ln\frac{\phi_{emi}}{< Q_{ei} >_{EL} \int_{E_g}^{\infty}\phi_{bb}(E)dE} \tag{4}$$

where $< Q_{ei} >_{EL}$ presents the average value of the EQE over the EL emission spectra. Fig. 4(a) shows three images of the internal voltage distribution over the solar cell's surface with forward injection current density of 7.5, 15, 37.5 mA/cm^2 according to (4). Here we assume the EQE is spatially uniform. Fig. 4(b) shows the internal voltage across the cell in the *x*-direction (as the dash arrow shows in the inset) under different forward injection current density. It is obviously to see that as the injection current density gradually increases, the voltage drop across the cell also increases, the voltage drop was considered mainly due to the sheet resistance of the top layer. Fig. 4(c) shows the internal voltage across the cell in the *y*-direction (as the dash arrow shows in the inset) under different forward injection current density. There is no obvious voltage drop across the *y*-direction for all the injection current densities. The small periodical waving of the voltage across the *y*-direction is due to the shading of light by the periodically distributed grid line electrodes. However, a relatively big valley was seen in Fig. 4(c) along the *y*-direction as the dash line rectangle shows, this is due to the broken of the grid electrode at the corresponding position on the surface of the cell where a line-shape region with low intensity along the *x*-direction could be seen obviously in the left images as the dash-line rectangle shows [27]. The voltage drop across the electrode broken region decreased with decreasing current density, which indicated the local series but not shunt resistance increased, since the effect of shunt resistance on the voltage is more pronounced for smaller injection current densities [29].

U. Rau [15] stated that a solar cell that has the theoretical maximum power conversion efficiency will also act as an LED with the maximum possible luminescence efficiency, the solar-cell EQE and the external EL quantum efficiency (η_{em}^{LED}) in LED operation were directly linked by a reciprocity relation. The EL quantum efficiency (η_{em}^{LED}) is defined as the ratio between the number of emitted

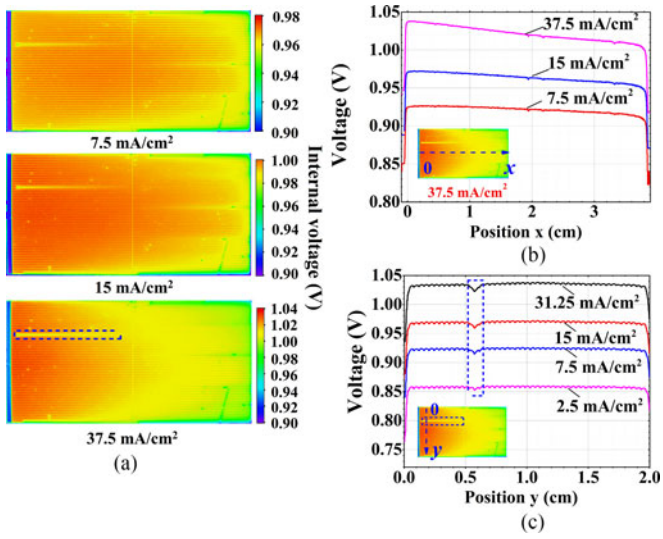

Fig. 4. (a) The internal voltage images of GaAs solar cell under forward injection current density of 7.5, 15 and 37.5 mA/cm^2,respectively. (b) Internal voltage across the cell in the x-direction as the dash arrow in the inset shows. (c) Internal voltage across the cell in the y-direction as the dash arrow in the inset shows.

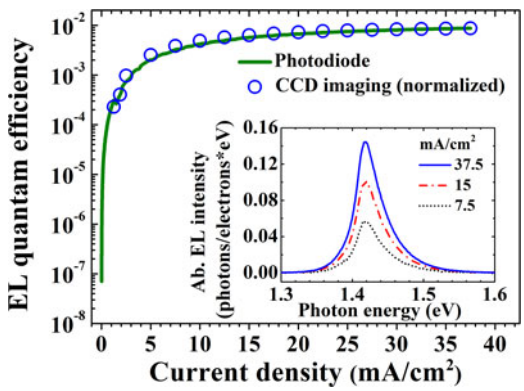

Fig. 5. EL quantum efficiency of the GaAs solar cell measured under LED operation as a function of the injection current density, both the results measured by Si-photodiode and CCD camera are presented. The inset is the absolute EL spectra divided by injection electron number for various injection current densities of the solar cell.

photons from the surface and the total injection electrons as follows,

$$\eta_{em}^{\mathrm{LED}} = \frac{\phi_{em}}{J_{inj}/q} \tag{5}$$

where ϕ_{em} (photons/(s·cm^2)) is the total emitted photon density from the top surface of the solar cell, J_{inj} is the injection current density. Fig. 5 shows the measured EL quantum efficiency as a function of the injection current density J_{inj}, the EL quantum efficiency was found to increase gradually with increasing injection current density, which indicates an increased radiative recombination rate at increased carrier densities [30]. In Fig. 5, both the results measured by Si-photodiode and CCD camera are presented, the EL intensity of CCD imaging was obtained by spatial integration of the CCD images and then the absolute value was calibrated by the Si-photodiode, then the EL quantum efficiency was calculated and the result coincided well with that measured by Si-photodiode which verified the reliability of the measurements. The inset shows the measured absolute EL spectra

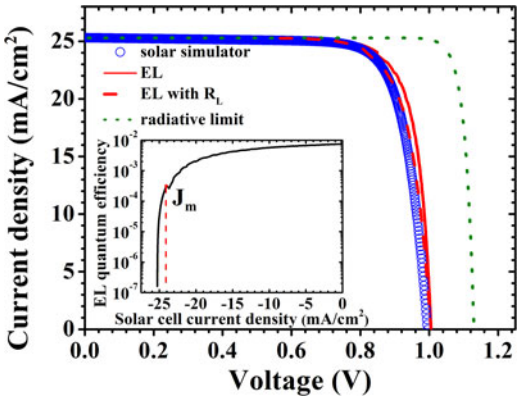

Fig. 6. I-V curves evaluated from EL measurement (the red solid line) and from I-V measurement with a solar simulator (the blue open circles). I-V curve measured by EL method after considering a lump resistance RL (the red dash dot line).

of the solar cell with various injection current density, the peak energy is around 1.42 eV which is estimated as the bandgap energy of the GaAs cell [25]. The EL quantum efficiency is obtained through the integrations of the EL peak in the absolute EL spectra.

The carrier-balance equation describing the optoelectronic processes in the solar cell irradiated with sunlight could be expressed as [25]

$$\phi_{sun} + J/q = \phi_{em} + \phi_{nr} \equiv (1/\eta_{em}{}^{LED})\phi_{em} \tag{6}$$

where $\phi_{sun} = \int Q_e(E) S_{AM1.5}(E) dE$ is the absorption rate of sunlight, $S_{AM1.5}$ is the standard AM1.5G solar spectrum; J is the current density (+ for forward injection current and – for photo-generated current); ϕ_{em} is the external radiative emission rate as above mentioned and was experimentally obtained using absolute EL measurments; ϕ_{nr} is the nonradiative recombination rate and η_{em}^{LED} is the EL quantum efficiency as above mentioned. According to the reciprocity relation between EL and EQE of a solar cell [15], the absolute EL emission rate ϕ_{em} is given by (2). The absolute EL emission rate ϕ_{em} as a function of the forward injection current density is experimentally measured. Therefore, the I-V curve of the solar cell could be predicted according to the equation:

$$V(I) = \frac{kT}{q} \ln \frac{\phi_{em}(I)}{< Q_e >_{EL} \int_{E_g}^{\infty} R_b(E) dE} \tag{7}$$

Based on the I-V curve extrapolated from the EL measurement, the essential photovoltaic parameters such as V_{oc}, FF, η and the maximum output voltage and current (V_m, J_m) could be obtained.

Fig. 6 shows the I-V curves evaluated from the absolute EL measurement (the red solid line) and from I-V measurement with a solar simulator (the blue open circles). The difference between the I-V curves measured by the two methods was considered mainly due to the effect of series resistance (R_s), which may originate from the cell itself including the resistance of the base bulk, the base contact and the external probe contact. The I-V curve measured by the EL method after considering a lump resistance R_L (the red dash dot line) is very close to the I-V curve measured with a solar simulator, here the value of R_L is estimated as $1\,\Omega\,\mathrm{cm}^2$. Also, the ideal I-V curve in the radiative recombination limit condition is shown (the green dot line), the difference between the I-V curve measured by the EL method and the I-V curve in the radiative limit is due to non-radiative recombination as following shows [14],

$$\Delta V = V_{rad} - V_{EL} = -\frac{kT}{q} \ln \eta_{em}^{\mathrm{LED}} \tag{8}$$

where the voltage loss ΔV between the voltage in the radiative limit (V_{rad}) and the voltage estimated from the EL measurement (V_{EL}) is related to the EL quantum efficiency (η_{em}^{LED}).

Table 1

Parameters of the GaAs Solar Cell Evaluated From the I-V Curves Obtained From I-V Measurement With Solar Simulator, From EL Measurement and From Radiative Limit Estimation

	V_{oc} (V)	J_{sc} (mA/cm^2)	V_m (V)	J_m (mA/cm^2)	FF	η
Solar simulator	0.996	25.3	0.845	22.96	0.767	19.4%
EL method	1.01	25.3	0.849	24.05	0.798	20.4%
Radiative limit	1.13	25.3	1.04	24.71	0.899	25.7%

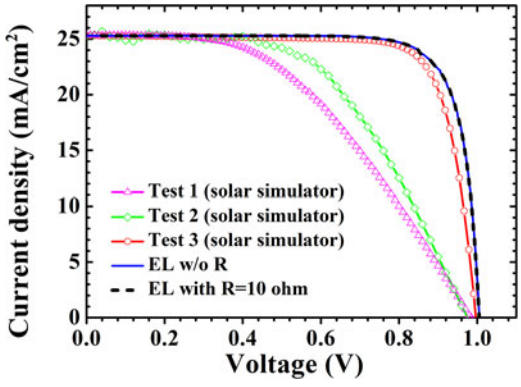

Fig. 7. I-V curves of the same GaAs solar cell measured under different condition and method, including with solar simulator system under different probe contact condition from test 1 to test 3 and with EL method without and with an artificial connected series resistor.

It is noted that the bending of the I-V curve near the maximum power point (J_m, V_m) is softer than that in the radiative limit, which lowers the filling factor, the soft bending in the EL I-V curve is considered to originate from the soft bending of the EL quantum efficiency curve near Jm as the inset in Fig. 6 shows. In other words, the soft bending is caused by the lowered luminescence quantum efficiency or radiative recombination efficiency at low carrier density and not by series resistance. Table 1 shows the basic parameters of the GaAs solar cell evaluated from the I-V curves obtained from I-V measurement with solar simulator, by EL method and from radiative limit estimation, respectively.

Actually, EL method has a merit over the traditional I-V measurement that it avoids the influence of the external parasitic resistance effect such as the series resistance due to the probe contact, which may affect the evaluation of the real parameters of the solar cell. For traditional I-V measurement, contact probes of high quality should be required. For common I-V measurement system especially in small laboratories without accurate calibration conditions, enormous difference due to different probe contact condition in different measurement system may occur. In Fig. 7, the IV curves from test 1 to test 3 is obtained from different IV measurement system in different small labs (with different probe contact condition) for the same solar cell sample, it is obviously to see the great inaccuracy due to the series resistance effect from external contact. To study the effect of series resistance on the I-V measurement by the EL method, a resistor of 10 Ω was artificial series-connected to the EL measurement system, that is, in addition to the contact probe. It can be seen that the series resistance has little influence on the I-V evaluation from the EL method, which also means that the series resistance caused by the probe contact could be ignored. The I-V measurement from EL method is especially reliable for parameters evaluation of solar cells with small internal series resistance since the series resistance caused by external probe contact could be neglected.

Table 2
Parameters of the GaAs Solar Cell Working at the Maximum-Output-Power Condition

	Input			Loss			
	AM1.5G	EM	NR	TR	TH	JN	Power output
GaAs cell	1.00	1.70E-3	0.062	0.462	0.148	0.132	0.194

All values are given in ratio.

The present measurements of EL efficiency and solar cell EQE also provided all the terms of emission loss, nonradiative loss processes in addition to the I-V curves. We evaluated all the loss/output rates in the solar cell under AM1.5G 1-sun irradiation under the working condition of maximum output power [25]. Table 2 shows the calculated parameters of the GaAs solar cell working at the maximum-output-power condition, including the energy gain and loss in the cell, and all the values are given in ratio. 19.4% of the solar energy is converted into electric energy, while the remainder goes into 0.17% radiative emission (EM) loss, 6.2% nonradiative recombination (NR) loss, 14.8% thermalization (TH) loss, 46.2% transmission (TR) loss and 13.2% junction (JN) loss. The contribution of radiative emission loss is negligibly small in the maximum-out-put-power condition. The calculated ratio of the output power 19.4% is identical with the measured cell efficiency of 19.4% as previous section shows, indicating the accuracy of the calculation.

4. Conclusion

In summary, an absolutely calibrated electroluminescence (EL) imaging method was utilized to investigate the properties of a GaAs thin-film solar cell. The distribution of the internal voltage of the solar cell and the sheet resistance of the window-layer of the solar cell were determined from the absolute EL measurements. Then, the I-V relation from the combination of the absolute EL and EQE measurements was extrapolated and was found to have a merit over the conventional I-V relation measured with a solar simulator that the series resistance effect caused by external probe contact could be eliminated. Finally, the optic-electro conversion losses of the solar cell including radiative loss, nonradiative loss, thermalization loss, transmission loss and junction loss were quantitatively determined from the EL and EQE measurements.

References

[1] T. Fuyuki, H. Kondo, T. Yamazaki, Y. Takahaschi, and Y. Uraoka, "Photographic surveying of minority carrier diffusion length in polycrystalline silicon solar cells by electroluminescence," *Appl. Phys. Lett.*, vol. 86, 2005, Art. no. 262108K.
[2] F. Fruehauf and M. Turek, "Quantification of electroluminescence measurements on modules," *Energy Procedia*, vol. 77, pp. 63–68, 2015.
[3] G. W. Shu *et al.*, "Optical coupling from InGaAs subcell to InGaP subcell in InGaP/InGaAs/Ge multi-junction solar cells," *Opt. Exp.*, vol. 21, pp. A123–A130, 2013.
[4] M. Seeland, R. Rösch, and H. Hoppe, "Quantitative analysis of electroluminescence images from polymer solar cells," *J. Appl. Phys.*, vol. 111, 2012, Art. no. 024505.
[5] Z. Hameiri *et al.*, "Photoluminescence and electroluminescence imaging of perovskite solar cells," *Progress Photovolt.*, vol. 23, pp. 1697–1705, 2015.
[6] M. Bokalič, J. Raguse, J. R. Sites, and M. Topič, "Analysis of electroluminescence images in small-area circular CdTe solar cells," *J. Appl. Phys.*, vol. 114, 2013, Art. no. 123102.
[7] B. Li, A. Stokes, and J. Doble, "Evaluation of two-dimensional electrical properties of photovoltaic modules using bias-dependent electroluminescence," *Progress Photovolt.*, vol. 20, pp. 936–944, 2012.

[8] P. Chaturvedi, H. Bram, and T. M. Walsh, "Broken metal fingers in silicon wafer solar cells and PV modules," *Sol. Energy Mater. Sol. Cells*, vol. 108, pp. 78–81, 2013.
[9] A. Kitiyanan *et al.*, "Comprehensive study of electroluminescence in multicrystalline silicon solar cells," *J. Appl. Phys.*, vol. 106, 2009, Art. no. 043717.
[10] M. Schneemann, T. Kirchartz, R. Carius, and U. Rau, "Measurement and modeling of reverse biased electroluminescence in multi-crystalline silicon solar cells," *J. Appl. Phys.*, vol. 114, 2013, Art. no. 134509.
[11] H. Nesswetter, W. Dyck, P. Lugli, A. W. Bett, and C. G. Zimmermann, "Luminescence based series resistance mapping of III-V multijunction solar cells," *J. Appl. Phys.*, vol. 114, 2013, Art. no. 194510.
[12] M. Seeland, C. Kästner, and H. Hoppe, "Quantitative evaluation of inhomogeneous device operation in thin film solar cells by luminescence imaging," *Appl. Phys. Lett.*, vol. 107, 2015, Art. no. 073302.
[13] K. Ramspeck, K. Bothe, D. Hinken, B. Fischer, J. Schmidt, and R. Brendel, "Recombination current and series resistance imaging of solar cells by combined luminescence and lock-in thermography," *Appl. Phys. Lett.*, vol. 90, 2007, Art. no. 153502.
[14] P. Wurfel, T. Trupke, T. Puzzer, E. Schaffer, W. Warta, and S. Glunz, "Diffusion lengths of silicon solar cells from luminescence images," *J. Appl. Phys.*, vol. 101, 2007, Art. no. 123110.
[15] U. Rau, "Reciprocity relation between photovoltaic quantum efficiency and electroluminescence emission of solar cells," *Phys. Rev. B*, vol. 76, 2007, Art. no. 085303.
[16] T. Kirchartz, A. Helbig, W. Reetz, M. Reuter, J. H. Werner, and U. Rau, "Reciprocity between electroluminescence and quantum efficiency used for the characterization of silicon solar cells," *Progress Photovolt.*, vol. 17, pp. 394–402, 2009.
[17] D. Hinken, K. Ramspeck, K. Bothe, B. Fischer, and R. Brendel, "Series resistance imaging of solar cells by voltage dependent electroluminescence," *Appl. Phys. Lett.*, vol. 91, 2007, Art. no. 182104.
[18] O. Breitenstein, J. Bauer, T. Trupke, and R. Bardos, "On the detection of shunts in silicon solar cells by photo- and electroluminescence imaging," *Progress Photovolt.*, vol. 16, pp. 325–330, 2008.
[19] T. Potthoff, K. Bothe, U. Eitner, D. Hinken, and M. Kontges, "Detection of the voltage distribution in photovoltaic modules by electroluminescence image," *Progress Photovolt.*, vol. 18, pp. 100–106, 2010.
[20] O. Breitenstein, A. Khanna, Y. Augarten, J. Bauer, J. M. Wagner, and K. Iwig, "Quantitative evaluation of electroluminescence images of solar cells," *Phys. Status Solidi (RRL)*, vol. 4, pp. 7–9, 2010.
[21] J. Haunschild, M. Glatthaar, M. Kasemann, S. Rein, and E. R. Weber, "Fast series resistance imaging for silicon solar cells using electroluminescence," *Phys. Status Solidi (RRL)*, vol. 3, pp. 227–229, 2009.
[22] H. Kampwerth, T. Trupke, J. W. Weber, and Y. Augarten, "Advanced luminescence based effective series resistance imaging of silicon solar cells," *Appl. Phys. Lett.*, vol. 93, 2008, Art. no. 202102.
[23] M. Glatthaar *et al.*, "Spatially resolved determination of the dark saturation current of silicon solar cells from electroluminescence images," *J. Appl. Phys.*, vol. 105, 2009, Art. no. 113110.
[24] M. Yoshita *et al.*, "Calibration standards and measurement accuracy of absolute electroluminescence and internal properties in multi-junction and arrayed solar cells," *Proc. SPIE*, vol. 9743, 2016, Art. no. 97430D.
[25] S. Q. Chen *et al.*, "Thorough subcells diagnosis in a multi-junction solar cell via absolute electroluminescence-efficiency measurements," *Sci. Rep.*, vol. 5, 2015, Art. no. 7836.
[26] T. Mochizuki *et al.*, "Solar-cell radiance standard for absolute electroluminescence measurements and open-circuit voltage mapping of silicon solar modules," *J. Appl. Phys.*, vol. 119, 2016, Art. no. 034501.
[27] T. Fuyuki and A. Kitiyanan, "Photographic diagnosis of crystalline silicon solar cells utilizing electroluminescence," *App. Phys. A*, vol. 96, pp. 189–196, 2009.
[28] G. T. Koishiyev and J. R. Sites, "Impact of sheet resistance on 2-D modeling of thin-film solar cells," *Sol. Energy Mater. Sol. Cells.*, vol. 93, pp. 350–354, 2009.
[29] A. Helbig, T. Kirchartz, R. Schaeffler, J. H. Werner, and U. Rau, "Quantitative electroluminescence analysis of resistive losses in Cu(In, Ga)Se_2 thin-film modules," *Sol. Energy Mater. Sol. Cells*, vol. 94, pp. 979–984, 2010.
[30] C. Jordan *et al.*, "Carrier-density dependence of the photoluminescence lifetimes in ZnCdSe/ZnSSe quantum wells at room temperature," *Appl. Phys. Lett.*, vol. 74, pp. 3359–3361, 1999.